Algorithm for radiometrically-accurate nonuniformity correction with arbitrary scene motion

Bradley M. Ratliff[a], Majeed M. Hayat,[b] and J. Scott Tyo[c]

University of New Mexico, Department of Electrical and Computer Engineering
Albuquerque, New Mexico 87131-1356

ABSTRACT

This paper describes a major generalization of a recently reported radiometrically-accurate algebraic nonuniformity correction (NUC) algorithm. The original technique was capable of accurately estimating the bias nonuniformity from a sequence of pairs of images exhibiting strictly one-dimensional (1D) subpixel shifts. The new technique relaxes the subpixel 1D shift constraint to arbitrary two-dimensional (2D) motion, which can be either sub-pixel or super-pixel. The 2D technique relies on calibrating only rows and columns on the perimeter of the array, which in turn, provides the algorithm with the necessary initial conditions to recursively estimate the bias values in the entire array. In this way, radiometric NUC can be achieved non-disruptively, as needed, without disturbing the functionality of the interior array elements. The 2D algorithm is highly localized in time and space lending itself to near real-time implementation. Radiometric NUC can be achieved with a relatively low number of frames (typically about 10 frame pairs). Moreover, as in its earlier 1D version, the performance of the 2D algorithm is shown to be insensitive to spatial diversity in the scene. This paper will address the performance of the 2D technique using real infrared data.

Keywords: nonuniformity correction, focal-plane array, infrared sensors, fixed-pattern noise, radiometric accuracy, calibration, scene-based NUC.

1. INTRODUCTION

Fixed-pattern noise, or spatial nonuniformity, remains a significant problem for focal-plane array (FPA) sensors despite considerable advances in technology over the years. Nonuniformity affects all FPA sensors, but it is particularly problematic for mid- to far-infrared (IR) detectors. Nonuniformity is mainly attributable to the differing photoresponses of each detector in the FPA.[1] Fluctuations in the environment surrounding the sensor as well as variation in transistor bias voltage of individual sensor photodetectors also contribute to the problem. Because of these time-varying conditions, the fixed-pattern noise drifts in time. Thus, a single factory-time calibration is ineffective.

There are two main classes of nonuniformity correction (NUC) techniques: those that are calibration-based and others that are scene-based. The most common calibration-based technique is the two-point calibration[2] (TPC). In TPC, normal operation of the imaging system is interrupted while the FPA stares at a calibration target. For IR systems, the target is typically a black-body radiation source that is heated to two different, known temperatures. Using these reference images, the nonuniformity parameters are solved for in a linear fashion. Two-point calibration yields radiometric images, but the procedure must be repeated relatively often as the nonuniformity parameters drift in time. Though the technique produces accurate radiometric imagery, the calibration equipment can be costly and it requires a significant amount of physical space.

In recent years, a considerable amount of research has been focused on the development of scene-based NUC techniques, which are algorithmic by nature. There are a wide variety of scene-based techniques. Some are statistical in nature, such as those presented by Narendra *et al.*,[3,4] Harris *et al,*[5,6] Chiang *et al,*[7] and more recently by Hayat *et al,*[8] and Torres *et al.*[9,10] Motion-based algorithms include those by O'Neil *et al,*[11,12] and Hardie *et al.*[13] A one-dimensional (1D) algebraic scene-based technique was developed by Ratliff *et al.*[14,15] Scene-based techniques are typically used in applications where radiometric accuracy is not required, as they

[a]bratliff@eece.unm.edu; [b] hayat@eece.unm.edu; phone (505) 277-0297; fax (505) 277-1439 [c] tyo@eece.unm.edu.

usually provide cosmetic image enhancement while compromising radiometric accuracy. Many scene-based techniques must be applied after the data has been acquired since some are computationally intensive and cannot be implemented in real time. Scene-based techniques do provide two major advantages over calibration-based techniques in that they do not require interrupting camera operation (by a calibration target) and they can typically be implemented cost-effectively in hardware or software.

In this paper, we present a major generalization to a recently reported 1D radiometrically-accurate scene-based NUC technique by Ratliff *et al.*.[16] Our earlier work[16] bridged scene-based and calibration-based techniques by utilizing a 1D algebraic scene-based technique[14, 15] in conjunction with a limited two-point calibration technique. Such integration allows an imaging system to produce radiometrically accurate imagery without interruption of the interior photodetectors of the FPA, thus providing the best of both types of techniques. The 1D radiometric technique, however, is restrictive in the sense that it can only make use of image pairs that exhibit subpixel 1D motion. Here, we present a major extension of this technique that allows for the inclusion of image pairs containing arbitrary two-dimensional (2D) motion. This extension is made possible precisely due to the perimeter calibration, which provides the necessary boundary conditions required by this new form of the algorithm. Hence, by calibrating rows and columns only along the perimeter of the FPA, via a two-point calibration, the 2D algebraic technique can transport the calibration of these perimeter detectors to interior, uncalibrated photodetectors. Therefore, this new radiometrically-accurate scene-based algorithm (RASBA) allows the interior FPA detectors to remain unobstructed while maintaining radiometrically accurate imagery. This paper presents some promising results of the 2D RASBA using real infrared data, along with a preliminary performance analysis.

This paper is organized as follows. The photodetector model and basic assumptions required by the 2D RASBA are presented in Section 2. Development of the 2D RASBA is discussed in Section 3. Experimental results are given in Section 4. Finally, conclusions and future avenues of research are given in Section 5.

2. MODEL

In this section we discuss the FPA model used by the two-point calibration and the simplified detector model used by the 2D RASBA. The basic assumptions imposed on the inter-frame scene motion, or shift, required by the 2D RASBA are also given.

2.1. Sensor Model

Consider an FPA sensor that generates an MxN image sequence y_n, where $n = 1, 2, 3, \ldots$, represents the image frame number. A commonly-used linear approximation for each FPA's output is given by

$$y_n(i,j) = a(i,j)z_n(i,j) + b(i,j), \tag{1}$$

where $z_n(i,j)$ is the irradiance (i.e. the average number of photons collected by the ijth detector), and $a(i,j)$ and $b(i,j)$ are the detector gain and bias, respectively. The standard two-point calibration makes use of this model, accounting for both gain and bias nonuniformity.

In some applications, bias nonuniformity dominates the gain nonuniformity; therefore, as a way to simplify the model of Eq. (1), the gain is assumed uniform across all detectors with a value of unity. Thus, the detector model becomes

$$y_n(i,j) = z_n(i,j) + b(i,j). \tag{2}$$

The 2D RASBA uses the above simplified model, and hence is a bias NUC algorithm.

2.2. Motion Model

The 2D RASBA assumes that the temperature of objects does not change during the time between image frames. Thus, when there is 2D motion between two adjacent image frames, we may decompose this motion into a vertical component, α, and a horizontal component, β. Each shift may be written as its whole-integer and fractional parts, i.e., $\alpha = \lfloor\alpha\rfloor + \Delta\alpha$ and $\beta = \lfloor\beta\rfloor + \Delta\beta$, where $\lfloor\cdot\rfloor$ indicates the integer part of the shift towards zero (e.g., $\lfloor 1.2\rfloor = 1$ and $\lfloor -2.2\rfloor = -2$). Thus, for a pair of image frames exhibiting a downward-α and

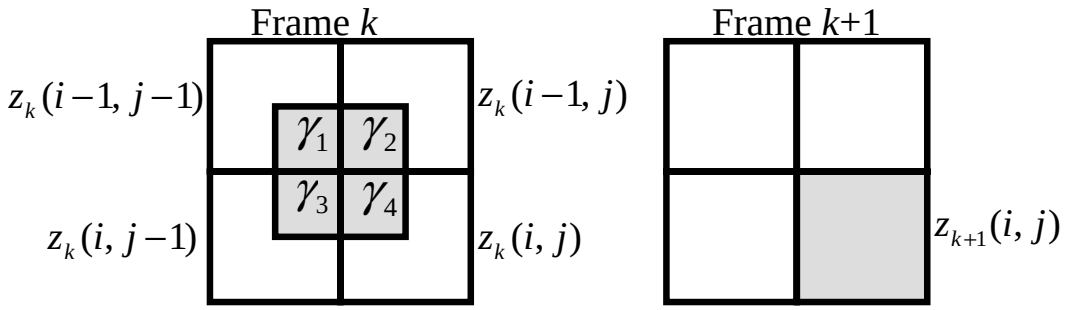

Figure 1. Graphical depiction of the linear interpolation model for subpixel 2D motion. The shaded pixels represents the interpolated irradiance value at time $k+1$.

rightward-β shift (we adopt the convention that downward vertical motion and rightward horizontal motion are positive), we may linearly interpolate four irradiance values from the kth frame to estimate the irradiance value in a corresponding pixel in the shifted $(k+1)$th frame. Hence, we model each $(k+1)$th detector response as

$$\begin{aligned} y_{k+1}(i,j) &= |\Delta\beta|\Big(|\Delta\alpha| z_k(i-\lfloor\alpha\rfloor-1, j-\lfloor\beta\rfloor-1) \\ &\quad + (1-|\Delta\alpha|) z_k(i-\lfloor\alpha\rfloor, j-\lfloor\beta\rfloor-1)\Big) \\ &\quad + (1-|\Delta\beta|)\Big(|\Delta\alpha| z_k(i-\lfloor\alpha\rfloor-1, j-\lfloor\beta\rfloor) \\ &\quad + (1-|\Delta\alpha|) z_k(i-\lfloor\alpha\rfloor, j-\lfloor\beta\rfloor)\Big) + b(i,j), \end{aligned} \tag{3}$$

where $i = 2+\lfloor\alpha\rfloor, 3+\lfloor\alpha\rfloor, \ldots, M$ and $j = 2+\lfloor\beta\rfloor, 3+\lfloor\beta\rfloor, \ldots, N$. If Eq. (3) is expanded, four multiplicative combinations of the fractional shift terms result. We define these constants as $\gamma_1 = |\Delta\alpha\Delta\beta|$, $\gamma_2 = (1-|\Delta\alpha|)|\Delta\beta|$, $\gamma_3 = |\Delta\alpha|(1-|\Delta\beta|)$, and $\gamma_4 = (1-|\Delta\alpha|)(1-|\Delta\beta|)$. Upon substitution of these terms, Eq. (3) becomes

$$\begin{aligned} y_{k+1}(i,j) &= \gamma_1 z_k(i-\lfloor\alpha\rfloor-1, j-\lfloor\beta\rfloor-1) \\ &\quad + \gamma_2 z_k(i-\lfloor\alpha\rfloor, j-\lfloor\beta\rfloor-1) \\ &\quad + \gamma_3 z_k(i-\lfloor\alpha\rfloor-1, j-\lfloor\beta\rfloor) \\ &\quad + \gamma_4 z_k(i-\lfloor\alpha\rfloor, j-\lfloor\beta\rfloor) + b(i,j). \end{aligned} \tag{4}$$

Figure (1) displays a graphical representation of this linear interpolation model. A pair of frames exhibiting motion in any of the three remaining directions may be modelled in an analogous fashion.

We next show how these models are used by the TPC and 2D RASBA to perform a radiometrically accurate scene-based NUC.

3. 2D RADIOMETRICALLY-ACCURATE SCENE-BASED TECHNIQUE

We now present the development of the 2D RASBA. For simplicity, we divide this new technique into two distinct phases, namely a calibration phase and an algorithmic phase. The calibration phase consists of a standard two-point calibration (though any calibration procedure may be substituted) with the exception that only detectors on the perimeter of the focal plane are calibrated, leaving other detectors unobstructed.

The algorithmic phase consists of the application of the 2D RASBA to the entire array. This algorithm is effectively able to "transport" the calibration of the perimeter detectors to the interior, uncalibrated detectors. We next present the details of each phase of this novel technique.

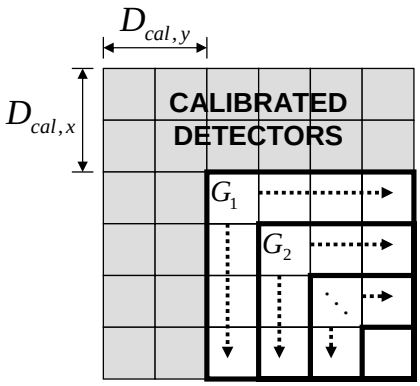

Figure 2. Graphical representation of the recursive operation of the algorithm. The bolded pixel partitions correspond to each G_ℓ, representing the group of detectors whose biases are estimated iteratively in ℓ. The arrows indicate the direction of algorithm iteration within each G_ℓ.

3.1. Calibration Phase

The calibration phase consists of a two-point calibration such that only detectors along the perimeter of the FPA are calibrated. We have designed an optical system that will do such a calibration and are currently in the process of implementing it. This calibration system will expose only perimeter detectors to the calibration target in such a way as to leave interior photodetectors unobstructed. Once the calibration target is in position, a TPC is performed (in the case of IR) by heating it to two different, known temperatures. For two distinct flat-field temperature values x_1 and x_2 at times k and $(k+m)$, respectively, and observed perimeter detector outputs $y_k(i,j)$ and $y_{k+m}(i,j)$, we find using Eq. (1)

$$a(i,j) = \frac{y_k(i,j) - y_{k+m}(i,j)}{x_1 - x_2} \tag{5}$$

and

$$b(i,j) = \frac{y_{k+m}(i,j)x_1 - y_k(i,j)x_2}{x_1 - x_2}. \tag{6}$$

With the gain and bias values known, each perimeter detector is calibrated using

$$\tilde{y}_k(i,j) = \frac{y_k(i,j) - b(i,j)}{a(i,j)}, \tag{7}$$

where $\tilde{y}_k(i,j)$ indicates a calibrated perimeter detector output. The shaded detectors in Fig. (2) depict the calibrated perimeter detectors, where $D_{cal,x}$ rows and $D_{cal,y}$ columns along the top and left side of the FPA, respectively, have been two-point calibrated. Realize that after calibration each perimeter detector ideally has a gain value of one and a bias equal to zero. Once the perimeter detectors have been successfully calibrated, the calibration target is removed from the camera FOV. It is important to note that since we have not yet built the calibration system, for the purposes of this paper, we perform a standard TPC and apply the gain and bias parameters only to perimeter outputs.

After calibration each perimeter detector will produce a radiometrically correct output. The uncalibrated detectors, on the other hand, continue to output raw data that are typically in a sampled form (i.e. 8-bit integer, 12-bit integer, etc). Since we make the assumption that each interior detector has a gain of unity, we first calculate the mean of all computed perimeter gain values. Next we simply divide each uncalibrated detector output by the this average gain value. It is important to note that this average gain is applied to each image before being processed by the 2D RASBA. At this point the algorithmic phase of the technique begins.

3.2. Algorithmic Phase

The algorithmic phase of the proposed technique consists of the application of the 2D RASBA. The main idea of the algorithm is to use pairs of consecutive image frames that exhibit a 2D shift in order to estimate the true bias nonuniformity. Given the proper initial conditions (obtained by calibrating the perimeter detectors), the resulting bias terms are manipulated so as to arrive at the radiometric bias value. We begin by computing a *bias differential* for an ijth detector by linearly combining four detector outputs from a kth frame with one detector output from a $(k+1)$th frame. More precisely, for two adjacent image frames exhibiting a down-rightward motion (the algorithm can analogously be extended to all types of motion), we compute a bias differential for the ijth detector by forming the linear combination

$$\begin{aligned}\Delta(i,j) &= \gamma_1 y_k(i-\lfloor\alpha\rfloor-1, j-\lfloor\beta\rfloor-1) \\ &\quad + \gamma_2 y_k(i-\lfloor\alpha\rfloor, j-\lfloor\beta\rfloor-1) \\ &\quad + \gamma_3 y_k(i-\lfloor\alpha\rfloor-1, j-\lfloor\beta\rfloor) \\ &\quad + \gamma_4 y_k(i-\lfloor\alpha\rfloor, j-\lfloor\beta\rfloor) - y_{k+1}(i,j). \end{aligned} \tag{8}$$

Now if we substitute Eqs. (2) and (4) into Eq. (8), all the irradiance terms in Eq. (8) will cancel, leaving a linear combination of only bias terms. Indeed,

$$\begin{aligned}\Delta(i,j) &= \gamma_1 b(i-\lfloor\alpha\rfloor-1, j-\lfloor\beta\rfloor-1) \\ &\quad + \gamma_2 b(i-\lfloor\alpha\rfloor, j-\lfloor\beta\rfloor-1) \\ &\quad + \gamma_3 b(i-\lfloor\alpha\rfloor-1, j-\lfloor\beta\rfloor) \\ &\quad + \gamma_4 b(i-\lfloor\alpha\rfloor, j-\lfloor\beta\rfloor) - b(i,j), \end{aligned} \tag{9}$$

where $i = 2+\lfloor\alpha\rfloor, 3+\lfloor\alpha\rfloor, \ldots, M$ and $j = 2+\lfloor\beta\rfloor, 3+\lfloor\beta\rfloor, \ldots, N$. Now suppose that we calibrate the top-most $\lfloor\alpha\rfloor$ rows and left-most $\lfloor\beta\rfloor$ columns of detectors, causing the perimeter detectors to have unity gain and zero bias. Observe that for the top-leftmost uncalibrated detector (i.e., for $i = \lfloor\alpha\rfloor+1$ and $j = \lfloor\beta\rfloor+1$), the differential bias $\Delta(\lfloor\alpha\rfloor+1, \lfloor\beta\rfloor+1)$ is precisely equal to $-b(i,j)$. Hence, we define the first bias estimate of the uncalibrated detectors as $\hat{b}(\lfloor\alpha\rfloor+1, \lfloor\beta\rfloor+1) = -\Delta(\lfloor\alpha\rfloor+1, \lfloor\beta\rfloor+1)$. Next we use Eq. (9) to progressively update each $\hat{b}(i,j)$ beyond $i = \lfloor\alpha\rfloor+1$ and $j = \lfloor\beta\rfloor+1$. The recursion in the algorithm starts (in the case of down-rightward motion) with the top-leftmost uncalibrated detector and proceeds in a downward and rightward manner, completing one row or column at a time. In this way, each bias value is progressively estimated until all array indexes have been exhausted.

From the above description of the algorithm, we observe that it has a recursive nature, and hence can be described more compactly as follows. Let $D_{cal,x}$ ($D_{cal,y}$) be the *calibration depth* of the FPA in the x (y) direction (i.e., the number of perimeter rows and columns of the FPA that have been absolutely calibrated). It is convenient to introduce the following partitioning of the pixels. For $\ell \geq \min(D_{cal,x}+1, D_{cal,y}+1)$ and $\ell \leq \min(M,N)$, define G_ℓ to represent the group of pixels consisting of $\{(\ell,\ell), \ldots, (M,\ell), (\ell,\ell+1), \ldots, (\ell,N)\}$, as depicted in Fig. (2). Note that such groups form a partition on all the uncalibrated detectors. The complete algorithm can now be stated as follows:

1. Initialization: For $i = 1, \ldots, D_{cal,x}$, $j = 1, \ldots, D_{cal,y}$, set $\hat{b}(i,j) = 0$. (From the perimeter calibration.)
2. Start the recursion: Put $\ell = \min(D_{cal,x}+1, D_{cal,y}+1)$, and estimate the biases in G_ℓ as follows. For $(i,j) \in G_\ell$,

$$\begin{aligned}\hat{b}(i,j) &= -\Delta(i,j) + \gamma_1\hat{b}(i-\lfloor\alpha\rfloor-1, j-\lfloor\beta\rfloor-1) + \gamma_2\hat{b}(i-\lfloor\alpha\rfloor, j-\lfloor\beta\rfloor-1) \\ &\quad + \gamma_3\hat{b}(i-\lfloor\alpha\rfloor-1, j-\lfloor\beta\rfloor) + \gamma_4\hat{b}(i-\lfloor\alpha\rfloor, j-\lfloor\beta\rfloor). \end{aligned} \tag{10}$$

3. Calculate the biases in $G_{\ell+1}$ according to the formula given by Eq. (10) for $(i,j) \in G_{\ell+1}$.
4. Repeat the previous step and terminate the recursion when $\ell = 1 + \min(M,N)$.

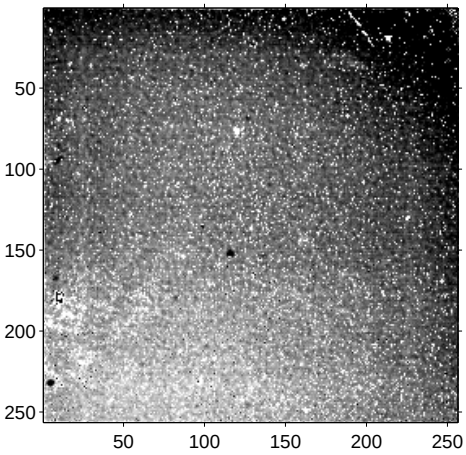

Figure 3. Flat field 323° Kelvin data sequence raw image frame 1.

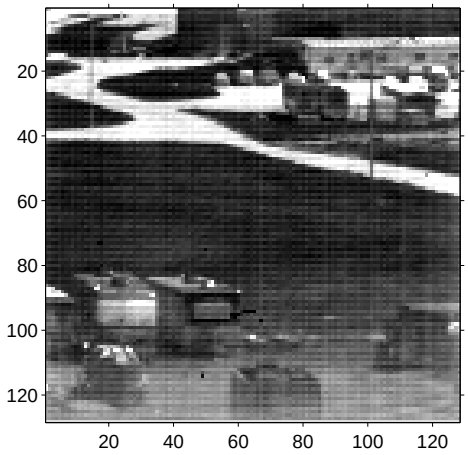

Figure 4. Scene data sequence raw image frame 1.

Note that when $\lfloor \alpha \rfloor = \lfloor \beta \rfloor = 0$, as in the case of subpixel motion, Eq. (10) simplifies to

$$\hat{b}(i,j) \quad = \quad \frac{1}{1-\gamma_4}\Big(-\Delta(i,j) + \gamma_1 \hat{b}(i-1,j-1) + \gamma_2 \hat{b}(i,j-1) + \gamma_3 \hat{b}(i-1,j)\Big). \tag{11}$$

An arbitrary raw image frame may now be corrected by simply subtracting each radiometric bias estimate from its corresponding detector output, yielding an estimate of the true irradiance, $\hat{z}_k(i,j) = y_k(i,j) - \hat{b}(i,j)$. Therefore, after correction, we are left with a radiometric image, with each corrected output ideally being of the form $\hat{z}_k(i,j) = z_k(i,j)$.

In the above derivation, down-rightward motion was assumed. To relax this assumption, an analogous recursive relationship may be derived for each of the remaining three motion categories. Moreover, to include all possible motion categories, detectors along the perimeter of the entire focal plane must be calibrated with an appropriate depth according to the maximum shift expected. We emphasize that the algorithm is able to handle both sub- and super-pixel 1D motion. In fact, if one motion component is zero and the other is subpixel, the algorithm reduces to the original 1D algorithm.[16]

Our studies have shown that estimation error in the motion parameters, α and β, can have a significant effect on the performance of the 1D algebraic technique.[15] This also holds for the 2D RASBA. For the results presented in this paper, a reliable gradient-based shift estimation algorithm[18,19] is employed to estimate all global motion. Shift estimation may be avoided if motion is known *a priori*, through precisely-controlled mechanical or optical means. A detailed analysis of the affect of shift estimation error on the 2D RASBA's performance, along with other pertinent performance issues may be found in Ratliff *et al.*[17]

As is widely known, spatial nonuniformity drifts slowly in time, requiring repeated focal plane calibration. Thus, as drift occurs, the perimeter detectors must be periodically re-calibrated. Doing so allows the 2D RASBA to maintain radiometric accuracy throughout sensor operation. In practice, the 2D RASBA is able to use many image pairs to estimate the bias nonuniformity. To decrease error in these radiometric estimates, the algorithm averages many of these estimates in time. The 2D RASBA employs an ensemble average of these estimates so that as the true nonuniformity of interior detectors change, the algorithm is able to capture nonuniformity drift. Results obtained from the 2D RASBA using real IR data are presented in the next section.

4. EXPERIMENTAL RESULTS

The degree to which the 2D RASBA is able to maintain radiometric accuracy was studied using real IR imagery. The data was collected from two different cameras. The first was a 12-bit 256x256 MgCdTe FPA camera (Amber

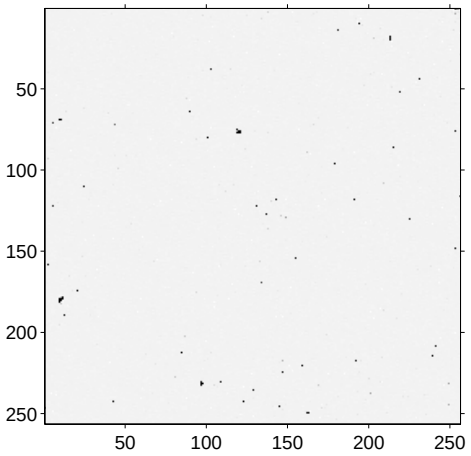

Figure 5. Flat field data sequence image frame 1 after two-point calibration; the dynamic range is 300° to 325° Kelvin.

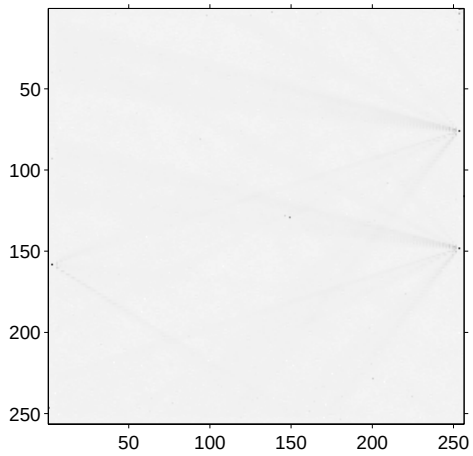

Figure 6. Flat field data sequence image frame 1 after correction by the 2D RASBA; the dynamic range is 300° to 325° Kelvin.

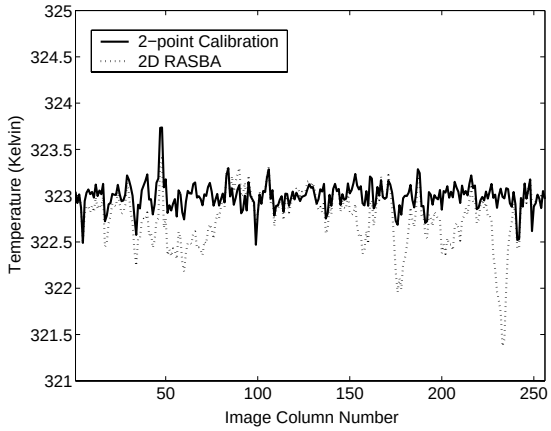

Figure 7. Raw corrected image output of frame 1, row 100 produced from both techniques for the flat field data sequence.

Mini-Dewer) operating in the long-wave IR 8.3-9.2 μm range (this data was collected at the Air Force Research Laboratory, NM). The second was a 12-bit 128x128 InSb FPA camera (Amber Model AE-4128) operating in the mid-wave IR 3-5 μm range (the data was generated at the Air Force Research Laboratory, OH).

The data sequence obtained from the MgCdTe camera was 256x256 by 64 frames and is of a flat-field calibration target heated to 323° Kelvin. The raw image frame 1 from the this image sequence is displayed in Fig. (3). The data sequence produced by the InSb camera was 128x128 by 512 frames. It was generated by randomly moving the camera by hand at an outdoor scene. The uncorrected frame 1 from this image sequence is displayed in Fig. (4). The severe amount of nonuniformity present in these raw images is clearly visible.

It is also important to note that before each of these image sequences were collected, two flat-field image sequences were obtained at two distinct temperatures. These flat-field image sequences were then used to perform a TPC. The nonuniformity parameters obtained from these TPC's were then used to calibrate the perimeter of each image sequence (with a calibration depth of 5). These "perimeter-calibrated" image sequences were next fed to and corrected by the 2D RASBA. Initial performance of the 2D RASBA was studied by comparing the corrected image sequences with those obtained from the standard TPC. The results obtained from these corrections are presented in the next two sections.

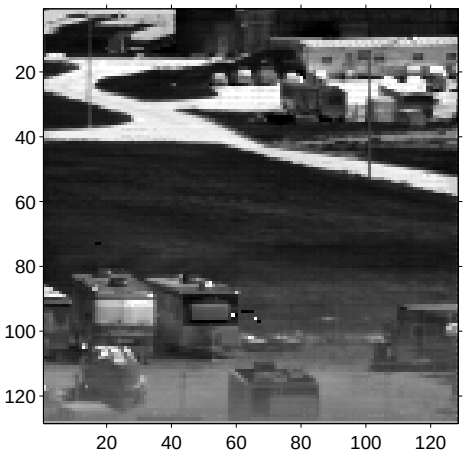

Figure 8. Scene data sequence image frame 1 after two-point calibration; the dynamic range is 280° to 340° Kelvin.

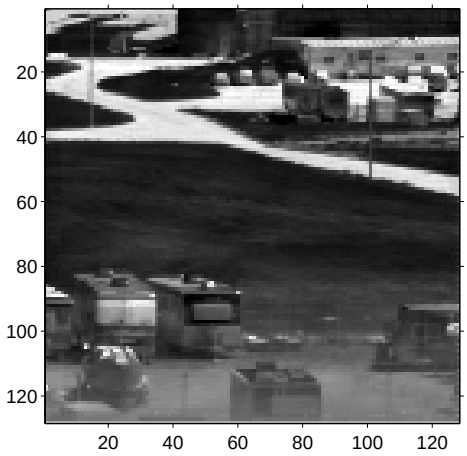

Figure 9. Scene data sequence image frame 1 after correction by the 2D RASBA; the dynamic range is 280° to 340° Kelvin.

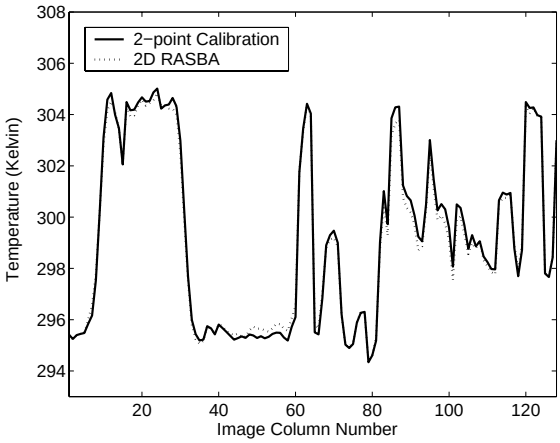

Figure 10. Raw corrected image output of frame 1, row 20 produced from both techniques for the scene data sequence.

4.1. Correction of Flat-field 323° Data Sequence

The flat field 323° data sequence was first corrected and studied. The reason for such a correction is to show several advantages of the 2D RASBA. First, it demonstrates the RASBA's insensitivity to spatial irradiance diversity. This is a notable property as most statistical techniques require a reasonable amount of irradiance diversity to produce a good correction. Second, because each image in the sequence is entirely uniform, motion becomes arbitrary and any sub-pixel value for the motion may be assumed. Thus, we may study RASBA performance in the presence of no shift estimation error. For the following correction, random uniformly distributed motion in the range of [-5, 5] pixels was used for all shift values.

The data sequence was first corrected using a two-point calibration, of which frame 1 is displayed in Fig. (5). Figure (6) displays image frame 1 after correction by the 2D RASBA. Examining the results of the TPC, the image is observed to be uniform, as expected, but a significant number of dead and flickering pixels are still noticeable. The image corrected by the 2D RASBA also appears uniform, but several faint lines emanating at varying angles from the right side of the image are visible. The reason for this is due to error in the calibration of perimeter pixels (i.e., dead or problematic detectors). Since 63 estimates of the bias nonuniformity were produced and averaged, the affect of this error is mitigated. These artifacts appear more prominent because

the dynamic range of the images is relatively small. It is also worth mentioning that the dead pixels present in the interior of the TPC image are not present in the 2D RASBA image, as the RASBA inherently does nearest neighbor pixel replacement. Overall, both images appear to be very similar.

To examine the level of radiometric accuracy achieved by the 2D RASBA, the raw corrected output of frame 1, row 100 from both corrected image sequences are plotted in Fig. (7). We observe that the results obtained from each correction are nearly identical, with both techniques producing outputs near the ideal value of 323° Kelvin. The NUC technique is thus producing a radiometric output.

4.2. Correction of Scene Data Sequence

The scene data sequence was next corrected and studied. A TPC was first performed on the data sequence. The TPC image frame 1 for this data sequence is displayed in Fig. (8). The perimeter of the scene data sequence was next calibrated and corrected by the 2D RASBA. Frame 1 resulting from this correction is shown in Fig. (9), scaled to the same dynamic range as the TPC image. It is important to note that in this correction image pairs exhibiting 1D motion as well as pairs with 2D shifts in the range $(-0.25, 0.25) \times (-0.25, 0.25)$ were omitted. The reason for this is due to the fact that in the case of small subpixel motion, the algorithm divides by these small shift values, and hence it has an adverse affect on the bias estimates (a detailed study of this phenomena, along with other pertinent performance issues, may be found in Ratliff *et al.*[17]). Hence, of the 511 image pairs, only 49 were used in the correction. The corrected outputs for frame 1, row 20 from the TPC and 2D RASBA-corrected scene data are displayed in Figure (10). Notice the high degree of accuracy demonstrated by the 2D RASBA, showing to be consistently within 0.5° Kelvin.

Visually comparing the TPC and RASBA-corrected images, we see that in both images the NU has effectively been removed. Notice that dead pixels persist in the TPC image whereas in the RASBA-corrected image they are largely suppressed. We again observe that the 2D RASBA has effectively obtained radiometric accuracy in the interior, uncalibrated detectors and is nearly identical to results obtained from a standard TPC.

5. CONCLUSIONS

We have presented a major extension to a recently reported technique for nonuniformity correction in focal plane arrays that combines a two-point calibration technique with an algebraic scene-based NUC algorithm. The resulting technique is able to provide radiometrically-accurate imagery without interruption of the imaging system field of view. Initial results of the technique appear promising, producing corrections that are nearly identical to those obtained from a standard two-point calibration. Future work will involve an intensive performance analysis as well as an effort to implement the 2D RASBA in lab.

ACKNOWLEDGMENTS

This research was supported by the National Science Foundation (CAREER Program MIP-9733308). We are grateful to Ernest Armstrong at the AFRL Sensors Directorate at Wright Patterson AFB, OH, and to Matthew Fetrow and David Bowers at the AFRL Space Vehicles Directorate at Kirland AFB, NM, for providing us with IR imagery.

REFERENCES

1. A. F. Milton, F. R. Barone, and M. R. Kruer, "Influence of nonuniformity on infrared focal plane array performance," Optical Engineering 24, pp. 855–862 (1985).
2. D. L. Perry and E. L. Dereniak, "Linear theory of nonuniformity correction in infrared staring sensors," Optical Engineering 32, pp. 1853–1859 (1993).
3. P. M. Narendra and N. A. Foss, "Shutterless fixed pattern noise correction for infrared imaging arrays," in Technical issues in focal plane development, W.S. Chan and E. Krikorian, eds., Proc. SPIE 282, pp. 44–51 (1981).
4. P. M. Narendra, "Reference-free nonuniformity compensation for IR imaging arrays," in Smart Sensors II, D.F. Barbe, ed., Proc. SPIE 252, pp. 10–17 (1980).

5. J. G. Harris, "Continuous-time calibration of VLSI sensors for gain and offset variations," in Smart Focal Plane Arrays and Focal Plane Array Testing, M. Wigdor and M.A. Massie, eds., Proc. SPIE 2474, pp. 23–33 (1995).
6. J. G. Harris and Y. M. Chiang, "Nonuniformity correction using constant average statistics constraint: Analog and digital implementations," in Infrared Technology and Applications XXIII, B.F. Andersen and M. Strojnik, eds., Proc. SPIE 3061, pp. 895–905 (1997).
7. Y. M. Chiang and J. G. Harris, "An analog integrated circuit for continuous-time gain and offset calibration of sensor arrays," Journal of Analog Integrated Circuits and Signal Processing 12, pp. 231–238 (1997).
8. M. M. Hayat, S. N. Torres, E. E. Armstrong and B. Yasuda, "Statistical algorithm for non-uniformity correction in focal-plane arrays," Applied Optics 38, pp. 772–780 (1999).
9. S. N. Torres, M. M. Hayat, E. E. Armstrong, and B. Yasuda, "A Kalman-filtering approach for non-uniformity correction in focal-plane array sensors," in Infrared Imaging Systems: Design, Analysis, Modeling, and Testing XI, G.C. Holst and JCD Publishing,eds., Proc. SPIE 4030, pp. 196–203 (2000).
10. S. N. Torres and M. M. Hayat, "Compensation for gain and bias nonuniformity and drift in array detectors: A Kalman-filtering approach," submitted to IEEE Transactions on Image Processing.
11. W. F. O'Neil, "Dithered scan detector compensation," in Proceedings of the 1993 International Meeting of the Infrared Information Symposium Specialty Group on Passive Sensors (Infrared Information Analysis Center, Ann Arbor, Michigan, 1993).
12. W. F. O'Neil, "Experimental verification of dithered scan nonuniformity correction," in Proceedings of the 1996 International Meeting of the Infrared Information Symposium Specialty Group on Passive Sensors (Infrared Information Analysis Center, Ann Arbor, Michigan, 1997), Vol. 1, pp. 329–339.
13. R. C. Hardie, M. M. Hayat, E. E. Armstrong and B. Yasuda, "Scene-based nonuniformity correction using video sequences and registration," Applied Optics 39, pp. 1241–1250 (2000).
14. B. M. Ratliff, M. M. Hayat, and R. C. Hardie, "Algebraic scene-based nonuniformity correction in focal-plane arrays," in *Infrared Imaging Systems: Design, Analysis, Modeling, and Testing XII*, G. C. Holst, ed., Proc. SPIE 4372, pp. 114–124 (2001).
15. B. M. Ratliff, M. M. Hayat, and R. C. Hardie, "An algebraic algorithm for nonuniformity correction in focal-plane arrays," JOSA A 19, pp. 1737–1747 (2002).
16. B. M. Ratliff, M. M. Hayat, and J. S. Tyo, "Radiometrically-calibrated scene-based nonuniformity correction for infrared array sensors," in *Infrared Technology and Applications XXVIII*, B. F. Anderson, G. F. Fulop, and M. Strojnik, eds., Proc. SPIE 4820, pp. 359–367 (2003).
17. B. M. Ratliff, M. M. Hayat, and J. S. Tyo, "Radiometrically-accurate scene-based nonuniformity correction for array sensors" JOSA A, submitted for publication.
18. M. Irani and S. Peleg, "Improving resolution by image registration," in Graph, Models and Image Process, CVGIP 53, pp. 231–239 (1991).
19. R. C. Hardie, K. J. Barnard, J. G. Bognar, and E. A. Watson, "High-resolution image reconstruction from a sequence of rotated and translated frames and its application to an infrared imaging system," Optical Engineering 37, pp. 247–260 (1998).